# Rewiring amino acid metabolism to boost nonnatural polyketide production in *Yarrowia lipolytica*

Jinpeng Wang[1,2#], Yuxiang Hong[1,3#], Zizhao Wu[1,4], Ayelet Fishman[2], Peng Xu[1,4, 5*]

[1]Department of Chemical Engineering, Guangdong Technion-Israel Institute of Technology (GTIIT), Shantou, Guangdong 515063, China

[2]Department of Biotechnology and Food Engineering, Technion-Israel Institute of Technology, Haifa, 3200003, Israel

[3]The Ruth and Bruce Rappaport Faculty of Medicine, Technion-Israel Institute of Technology, Haifa 320002, Israel

[4]Department of Chemical Engineering, Technion – Israel Institute of Technology, Haifa 32000, Israel

[5]Center for Lipid Engineering, Muyuan Laboratory, Zhengzhou, Henan 450016, China

*Corresponding author. P.X. (peng.xu@gtiit.edu.cn or peng.xu@technion.ac.il)

[#]These authors contribute equally to this article.

## Abstract

Malonyl-CoA is a central precursor involved in the synthesis of various bio-based chemicals, including polyketides, fatty acids and flavonoids. However, the production of these chemicals is often limited by the availability of malonyl-CoA. Based on retrosynthesis principles, we designed two thermodynamically favorable malonyl-CoA pathways using L-glutamate and L-aspartate as substrates. The novel pathways leverage oxidative deamination and decarboxylation reactions and efficiently channel metabolic flux toward malonyl-CoA, leading to increased triacetic acid lactone (TAL) production beyond the capability of the native acetyl-CoA carboxylase. We also discovered a new-to-nature polyketide (4-hydroxy-6-hydroxyethyl-2-pyrone) derived from the side activity of TAL pathway, reaching 5.4 g/L. This work highlights the utility of the novel malonyl-CoA pathways in enhancing polyketide production, and the possibility of using abundant amino acids or protein waste as feedstock to produce high-value nonnatural polyketides.

**Keywords:** Polyketides, Malonyl-CoA, L-Glutamate, L-Aspartate, Metabolic engineering, *Yarrowia lipolytica*

## Significance Statement

We engineered two thermodynamically favorable malonyl-CoA pathways in *Yarrowia lipolytica* using L-glutamate and L-aspartate as substrates. These pathways circumvent ATP dependency by leveraging oxidative deamination and decarboxylation reactions, offering a thermodynamically-favorable routes for bioproduction from abundant amino acids and waste proteins. The novel pathways outperformed the canonical acetyl-CoA carboxylase pathway in polyketide production, achieving up to moe than 3.7 g/L of triacetic acid lactone and a new-to-nature polyketide, 4-hydroxy-6-hydroxyethyl-2-pyrone (HHEP), at 5.4 g/L in bioreactor. The discovery of HHEP, a structural analog of kojic acid (a strong antimicrobial and skincare ingredient), underscores the potential of microbial cells for generating novel bioactive molecules. Our work highlights the interplay between pathway thermodynamics, enzyme kinetics, and metabolic flux redirection.

## 1. Introduction

Malonyl-CoA is the $C_2$ building block in the biosynthetic pathway of fats (*1, 2*), oleochemicals (*3*), and polyketides (*4-6*) in nature. As such, it sits at the heart of central metabolism in both prokaryotes and eukaryotes and underpins a vast range of biochemical transformations. Beyond its well-known role in fatty acid biosynthesis, malonyl-CoA is also integral to the biosynthesis of numerous high-value compounds including flavonoids (*7, 8*) and many pharmaceutically relevant polyketides (*9-13*). Consequently, boosting intracellular malonyl-CoA availability has become a central goal in metabolic engineering (*14, 15*).

Given malonyl-CoA's central importance, the quest for efficient and feasible malonyl-CoA pathways has long been a focus of the metabolic engineering community. The canonical route relies on pyruvate dehydrogenase (PDH) converting pyruvate into acetyl-CoA, followed by acetyl-CoA carboxylase (ACC) converting acetyl-CoA into malonyl-CoA (*16*). Although widely employed in industrial microorganisms, this PDH–ACC pathway carries a moderate overall negative Gibbs free energy ($\Delta_rG^{m\prime} \approx -51$ kJ/mol) yet also entails high ATP consumption. A second strategy uses malonyl-CoA synthetase (MCS) (*17-19*) to directly activate malonate into malonyl-CoA ($\Delta_rG^{m\prime} \approx -53.4$ kJ/mol), avoiding the carboxylation step and offering kinetic advantages due to simpler enzyme regulation. However, the cost of malonate is economically prohibitive. This route also imposes the cells high consumption of ATP. Recently, an alternative "transaminase–malonyl-CoA reductase" route was introduced to improve polyketide synthesis (*20*) in *E. coli*, wherein malonate semialdehyde (arising via transamination from β-alanine) is converted to malonyl-CoA by a specialized malonyl-CoA reductase. Although Gibbs energy for this emerging pathway ($\Delta_rG^{\circ\prime} \approx -16$ kJ/mol for the enzyme cascade) can be favorable under standard conditions (species concentration of 1 M), the standard Gibbs free energy under physiologically-relevant conditions ($\Delta_rG^{m\prime} \approx +0.6$ kJ/mol, species concentration of 1 mM) is thermodynamically unfavorable. In addition, existing enzyme pairs of transaminase and reductase demonstrated mediocre $K_m$ and $k_{cat}$ values. This necessitates us to find alternative malonyl-CoA pathways to improve microbial production of important metabolites.

An ideal malonyl-CoA pathway should offer greater thermodynamic favorability, improved catalytic constants, or less stringent cofactor and ATP requirements. In this study, we addressed this challenge by retro-synthetically designing and implementing

86 two novel malonyl-CoA routes, starting from the abundant amino acids L-glutamate
87 and L-aspartate. Both pathways leverage malonate semialdehyde as the intermediate
88 and malonyl-CoA reductase as a key step. Using the simplest polyketide TAL as a test
89 molecule, we experimentally validated that these new pathways efficiently redirect
90 carbon flux toward malonyl-CoA, and boosted TAL and a new-to-nature (4-hydroxy-6-
91 hydroxyethyl-2-pyrone) polyketide production in *Y. lipolytica*. Our re-designed
92 malonyl-CoA pathways expanded the biotechnological repertoire of high-value
93 polyketides from low-cost and abundant amino acids.

## 94 2. Results and discussion

### 95 2.1 Designing novel oxygen-dependent malonyl-CoA pathways from two abundant
### 96 amino acids

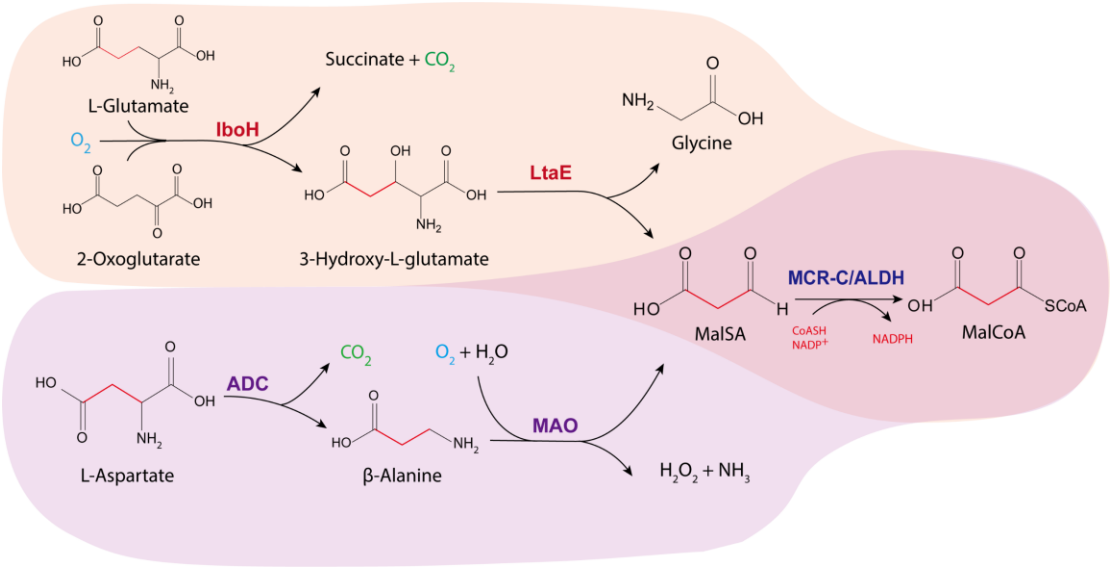


97

98 **Fig. 1** Novel $O_2$-dependent malonyl-CoA pathways derived from L-glutamate (upper
99 panel, ILM route) and L-aspartate (lower panel, AMM route). IboH: 2-oxoglutarate-
100 dependent L-glutamate dioxygenase; LtaE: aldolase; ADC: aspartate decarboxylase,
101 MAO: monoamine oxidase; MCR: malonyl-CoA reductase; ALDH: CoA-acylating
102 aldehyde dehydrogenase; MalSA: malonate semialdehyde; MalCoA: malonyl-CoA.

103 We began by applying a retrosynthetic framework to identify possible malonyl-
104 CoA pathways from two abundant amino acids, L-glutamate and L-aspartate. Both
105 proposed pathways generate malonate semialdehyde (MalSA) as an intermediate
106 and then employ malonyl-CoA reductase (MCR) to convert MalSA to malonyl-CoA
107 (**Fig. 1**). In the L-glutamate route, L-glutamate dioxygenase (IboH) (*21*) hydroxylates L-
108 glutamate to form 3-hydroxy-L-glutamate, which subsequently undergoes an aldol

cleavage (*22*), yielding MalSA and glycine. In the L-aspartate route, aspartate decarboxylase (ADC) converts L-aspartate to β-alanine (*23*), then β-alanine undergoes an oxidative deamination to form MalSA by a monoamine oxidase (MAO) (*24*), generating hydrogen peroxide ($H_2O_2$) as byproduct. Both enzymes rely on oxidative deamination and decarboxylation steps releasing $CO_2$, amine (or glycine) or $H_2O_2$, proceeding with increased entropy or disorder, signifying a strong driving force or large negative Gibbs energy change.

With an AI-powered kinetic data prediction tool UniKP (*25*) including reported kinetic data, and biochemical reaction thermodynamic calculator *eQuilibrator 3.0* (*26*), we retrieved the kinetic and thermodynamic information of the novel malonyl-CoA pathways. Compared to the canonical PDH-ACC and MCS routes, both the L-glutamate and L-aspartate pathways exhibit reduced ATP demand (**Table 1**), thereby impose less cellular energy cost. Thermodynamic and kinetic analyses (**Table 2**) indicate that although both pathways rely on MCR — known to exhibit marginal thermodynamic favorability on its own, the large driving force by coupling with oxidative deamination and decarboxylation steps will thermodynamically benefit MCR. Specifically, IboH-aldolase ($\Delta_rG^{m\prime} \approx -466.6$ kJ/mol) or ADC-MAO ($\Delta_rG^{m\prime} \approx -146.3$ kJ/mol) reactions each display large negative Gibbs free energy changes (**Table 2**), which collectively drive the overall pathway into a highly exergonic regime even when the MCR step by itself is relatively less favorable (*27-29*). This thermodynamic synergy sets our proposed pathways apart from the previously reported transaminase-MCR approach (*20*), whose net Gibbs energy under physiological conditions becomes slightly positive ($\Delta_rG^{m\prime} \approx +0.6$ kJ/mol). Moreover, preliminary $K_m$ and $k_{cat}$ values for IboH, aldolase, MAO, and MCR, fall within ranges better suitable for metabolic engineering (**Table 2**), than the transaminase-MCR route (*20*).

### 2.2 2PS produces TAL and an unknown metabolite from malonyl-CoA

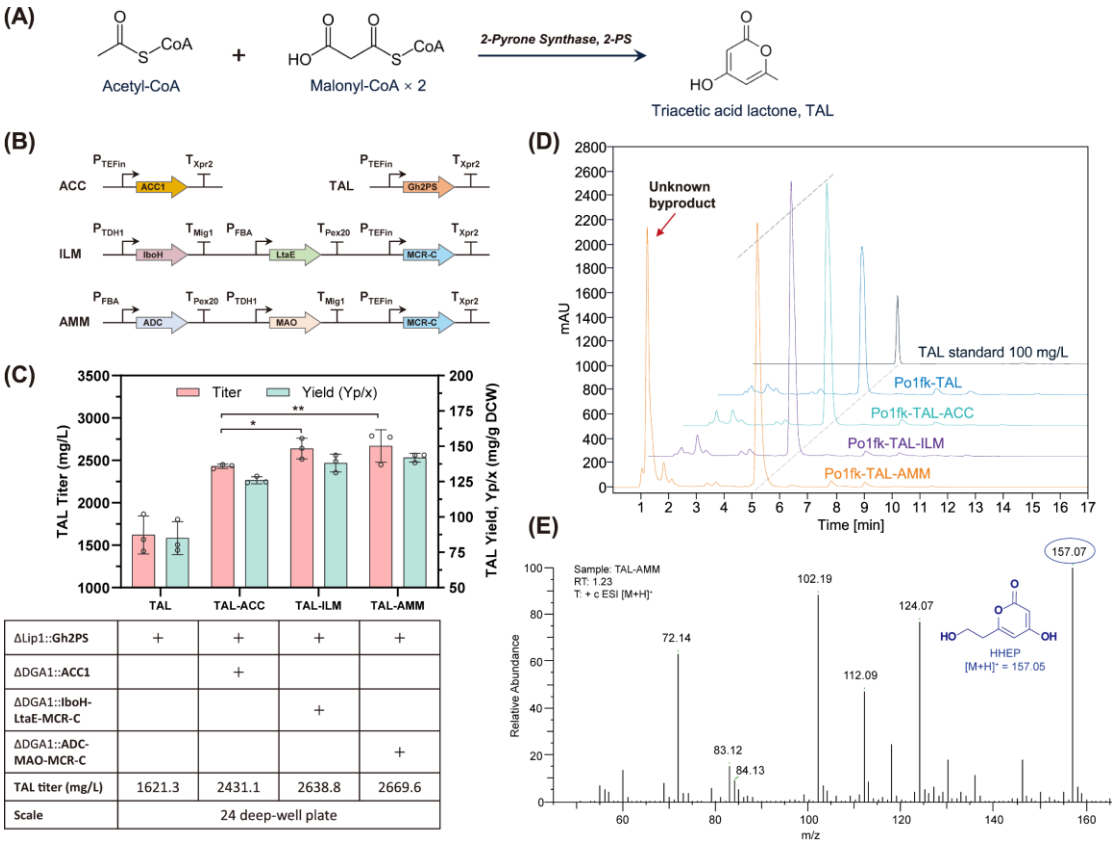


| | TAL | TAL-ACC | TAL-ILM | TAL-AMM |
|---|---|---|---|---|
| ΔLip1::Gh2PS | + | + | + | + |
| ΔDGA1::ACC1 | | + | | |
| ΔDGA1::IboH-LtaE-MCR-C | | | + | |
| ΔDGA1::ADC-MAO-MCR-C | | | | + |
| TAL titer (mg/L) | 1621.3 | 2431.1 | 2638.8 | 2669.6 |
| Scale | 24 deep-well plate | | | |

**Fig. 2** Testing the functionality of the novel malonyl-CoA pathways. (**A**) The simplest polyketide pathway encoded by 2-pyrone synthase (2-PS) was used as a reporter molecule; (**B**) Three TAL pathways, TAL-ACC, TAL-ILM and TAL-AMM tested in this work; (**C**) TAL titer and specific TAL yield from the engineered strains in deep-well plates. Experiments were performed in triplicate and the data is reported as mean ± SD. ** indicates statistically highly significant ($p < 0.01$), * indicates statistically significant ($p < 0.05$); (**D**) HPLC profile of TAL and an unknown by-product from the engineered strains; (**E**) LC-MS spectra of the unknown byproduct from the TAL-AMM strain.

We next validated whether the novel malonyl-CoA pathways can enhance polyketide production in *Y. lipolytica*. Using the simplest polyketide (triacetic acid lactone) as the test molecule, we integrated a codon-optimized 2-pyrone synthase (*Gh*2PS) from *Gerbera hybrida* (*30, 31*) into the *lip1* locus of *Y. lipolytica* Po1fk. This enzyme catalyzes the condensation of malonyl-CoA with acetyl-CoA (**Fig. 2A**) to form triacetic acid lactone (TAL), serving as a direct reporter for the newly designed malonyl-CoA pathways. To compare the performance of the novel pathways, we constructed three different strains (**Fig. 2B**) by integrating either ACC1 (canonical pathway), the ILM pathway (IboH-LtaE-MCR, using L-glutamate as substrate, **Fig. 1**),

155 or the AMM pathway (ADC-MAO-MCR, using L-aspartate as substrate, **Fig. 1**) into the
156 *DGA1* locus under well-defined promoters (Fig. 2B).

157 TAL production in deep-well plate cultures (**Fig. 2C**) indicates that both ILM and
158 AMM pathways outperformed the canonical ACC1 route in terms of titer and specific
159 yield (mgTAL/gDCW). Specifically, the strain carrying the ILM pathway achieved a TAL
160 titer of 2638.8 mg/L, while the AMM pathway led to a slightly higher TAL titer of
161 2669.6 mg/L (**Fig. 2C**), both exceeding the ACC1 control (2431.1 mg/L). This suggests
162 that the oxidative deamination and decarboxylation steps in the novel pathways (**Fig.**
163 **1**) effectively converted the amino acid precursors into malonyl-CoA, overcoming the
164 inherent limitations of ATP-dependent carboxylation in the ACC1 pathway (**Table 1**).
165 The higher TAL yield observed in the AMM pathway could be attributed to a more
166 favorable kinetic profile of the ADC-MAO cascade (**Table 2**). However, in baffled
167 flasks, AMM strain produced less TAL than the strain carrying ILM pathway
168 (**supplementary Fig. S1A**), possibly due to the accumulation of hydrogen peroxide
169 ($H_2O_2$) in the AMM pathway (**Fig. 1**).

170 Interestingly, HPLC analysis revealed an unknown by-product in the strain
171 carrying the AMM pathway (**Fig. 2D**). This unknown peak persists in the shaking flask
172 culture (**supplementary Fig. S1B**). This byproduct is likely derived from the β-alanine
173 or MalSA intermediates. We next identified the structure of the unknown peak (**Fig.**
174 **2D**) observed in the AMM strain. LC–MS analysis (**Fig. 2E**) revealed a major species
175 eluting at 1.26 min (**supplementary Fig. S2**), with a molecular weight of 157 Dalton
176 and characteristic fragmentation ions at $m/z = 124$, 112, 102, 84 and 72 under
177 positive (M+1) ionization modes. By comparing these fragmentation patterns against
178 standard databases and predicted mass spectra (**supplementary Fig. S3**), we
179 characterized this molecule as 4-hydroxy-6-hydroxyethyl-2-pyrone (HHEP) with a
180 chemical formula $C_7H_8O_4$.

181 **2.3 3-HP-CoA serves as the priming unit for the nonnatural polyketide HHEP**

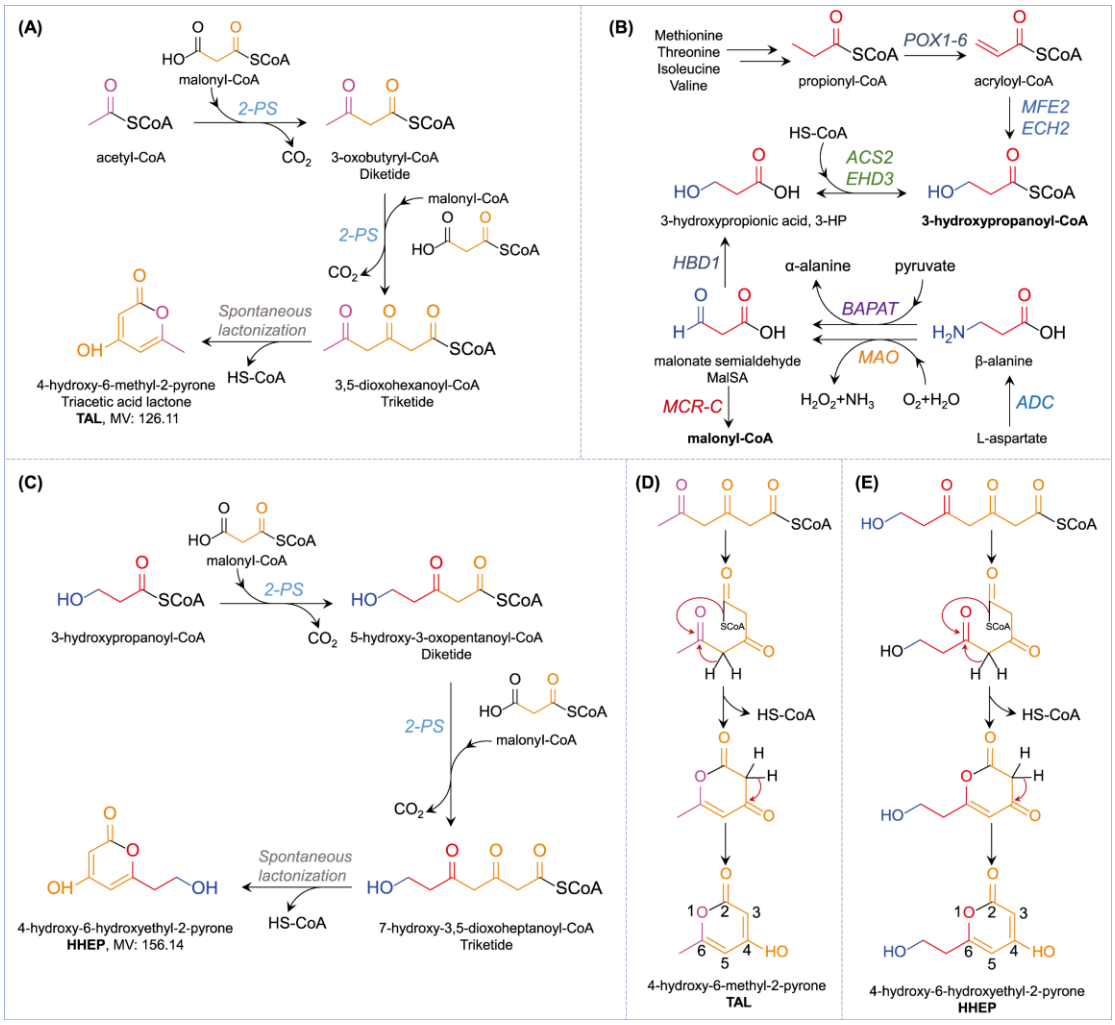


**Fig. 3**. Deciphering the biosynthetic route of the nonnatural polyketide HHEP. (**A**) Biosynthetic route of TAL by 2PS. (**B**) Generation of 3HP and 3HP-CoA from endogenous amino acid metabolism (upper panel) and β-alanine from L-aspartate decarboxylation (lower panel). BAPAT: β-alanine-pyruvate aminotransferase; MAO: monoamine oxidase; HBD1: 3-hydroxyacyl-CoA dehydrogenase; ACS2/EHD3: 3-hydroxypropanoyl-CoA synthetase; POX1-6: Fatty-acyl-CoA oxidase; MFE2: Multifunctional β-oxidation enzyme, hydratase/dehydrogenase; ECH2: Enoyl-CoA hydratase. (**C**) 3HP-CoA serves as a priming molecule to synthesize HHEP by 2PS. Spontaneous lactonization of triketide intermediates leads to the formation of triacetic acid lactone (**D**) and 4-hydroxy-6-hydroxyethyl-2-pyrone (**E**).

Interestingly, we found HHEP was synthesized in all the strains expressing 2PS (**Fig. 2D**, **supplementary Fig. S4** for ILM-TAL strain and **supplementary Fig. S5** for TAL strain), albeit HHEP was mostly accumulated in the AMM strain (**supplementary Fig. S1B** and **Fig. S2**). The non-exclusive production of HHEP from all the tested strains suggests that HHEP was derived from the downstream reactions of β-alanine.

198 Previously, the β-alanine pathway has been identified as the most economically-
199 attractive route to synthesize 3-hydroxypropionate (3HP) (*32*). Inspection of TAL
200 biosynthetic mechanism (**Fig. 3A**) indicated that HHEP was indeed generated as a
201 polyketide by-product when 3-hydroxypropanoyl-CoA (3HP-CoA) was used as the
202 priming molecule for 2-pyrone synthase (2PS) (**Fig. 3B** and **3C**) (*33*). In the AMM
203 strain, β-alanine generated from aspartate decarboxylase (ADC) can be oxidized to
204 form MalSA, which further is reduced to 3HP by host enzyme HBD1 encoding 3-
205 hydroxyacyl-CoA dehydrogenase (**Fig. 3B** lower panel). In fact, 3HP-CoA is also the
206 degradation product of methionine, threonine, leucine and valine (**Fig. 3A** upper
207 panel) from the media containing YPD and peptone. When we blasted the genome of
208 *Y. lipolytica*, we identified that at least one gene (YALI0D06325) encodes an enzyme
209 highly conserved with BAPAT encoding alanine aminotransferase which converts β-
210 alanine to MalSA (**supplementary Fig. S6**); and likewise, YALI0C08811 and
211 YALI0F05962/YALI0D06215g are highly conserved with HBD1 encoding 3-hydroxyacyl-
212 CoA dehydrogenase, and ACS2/EHD3 encoding 3-hydroxypropanoyl-CoA synthetase
213 (**supplementary Fig. S7-S9**), respectively. When 2PS encounters 3HP-CoA as a
214 priming unit, it will condense with two molecules of malonyl-CoA to form a
215 hydroxymethyl triketide intermediate (**Fig. 3C**). This intermediate, undergoes a series
216 of intramolecular nucleophilic substitutions and spontaneous lactonization,
217 ultimately cyclizes and rearranges to yield the more stable lactone 4-hydroxy-6-
218 hydroxyethyl-2-pyrone (HHEP) (**Fig. 3E**) following a similar pattern as 4-hydroxy-6-
219 methyl-2-pyrone (TAL) (**Fig. 3D**) does.

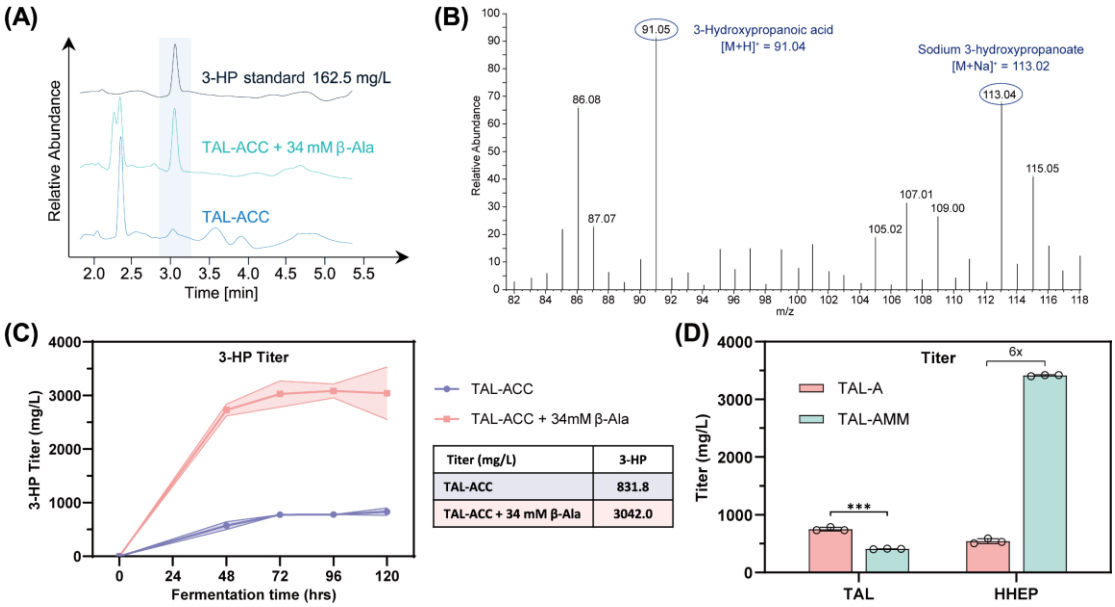


220

221 **Fig. 4** Validating 3-HP as an intermediate for HHEP synthesis. (**A**) HPLC profile of 3-HP

222 in the TAL-ACC strain with feeding of 34 mM β-alanine; (**B**) LC-MS characterization of
223 3HP in the TAL-ACC strain; (**C**) Production of 3HP in the TAL-ACC strain with or
224 without feeding of 34 mM β-alanine in shaking flasks; (**D**) TAL and HHEP production
225 in the TAL-A and TAL-AMM strain after 48 hours of fermentation in deep-well plates.
226 TAL-A is the strain with expression of 2PS and ADC. TAL-AMM is the strain with
227 expression of 2PS and the entire AMM pathway.

228 To validate that HHEP is derived from 3HP, we next fed 34 mM β-alanine to the
229 TAL-ACC strain and observed a substantially increased level of 3HP in deep-well
230 plates (Fig. **4A** and **supplementary Fig. S10A**) and HHEP (**supplementary Fig. S10B**).
231 The presence of 3HP was also confirmed by LC-MS analysis (**Fig. 4B**). For example,
232 TAL-ACC strain produced 3042.0 mg/L of 3HP with feeding of 34 mM β-alanine, more
233 than 3-fold higher than the same strain without feeding of β-alanine (831.8 mg/L)
234 (**Fig. 4C** and **supplementary Fig. S10A**). These facts confirm that endogenous BAPAT
235 (YALI0D06325) and HBD1 (YALI0C08811) can convert β-alanine to 3HP (**Fig. 3B**).
236 When only ADC was expressed, the TAL-A strain produced basal level of TAL (751.0
237 mg/L) and HHPE (542.4 mg/L) (**Fig. 4D** and **supplementary Fig. S10C**). However,
238 when the entire AMM pathway was expressed, the TAL-AMM strain produced 6-fold
239 more HHPE (3415.1 mg/L) compared to the TAL-A strain (**Fig. 4D** and **Supplementary**
240 **Fig. S10C**). This result showcases the critical roles of monoamine oxidase and MCR to
241 boost intracellular malonyl-CoA and improve HHEP synthesis (**Fig. 3B** and **Fig. 3C**).
242 The discrepancy of TAL and HHEP titer enhancement indicates the intracellular
243 scarcity of acetyl-CoA relative to 3-hydroxypropanoyl-CoA in the TAL-AMM strain.
244 Taken together, these results confirm that HHEP arises as a nonnatural polyketide by-
245 product when 3HP-CoA participates in the 2-PS condensation reaction (**Fig. 3B** and
246 **Fig. 3C**).

247 **2.4 Feeding amino acids to boost polyketide production in shaking flask**

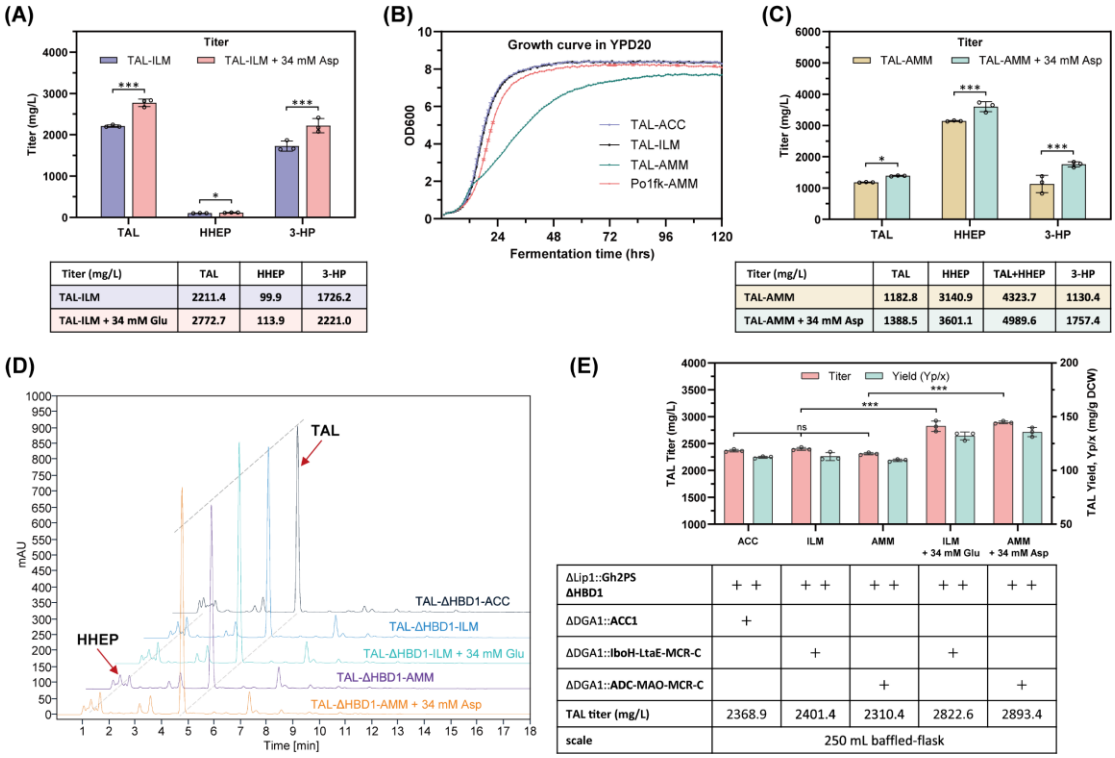


| Titer (mg/L) | TAL | HHEP | 3-HP |
|---|---|---|---|
| TAL-ILM | 2211.4 | 99.9 | 1726.2 |
| TAL-ILM + 34 mM Glu | 2772.7 | 113.9 | 2221.0 |

| Titer (mg/L) | TAL | HHEP | TAL+HHEP | 3-HP |
|---|---|---|---|---|
| TAL-AMM | 1182.8 | 3140.9 | 4323.7 | 1130.4 |
| TAL-AMM + 34 mM Asp | 1388.5 | 3601.1 | 4989.6 | 1757.4 |

| | | | | | |
|---|---|---|---|---|---|
| ΔLip1::Gh2PS ΔHBD1 | + + | + + | + + | + + | + + |
| ΔDGA1::ACC1 | + | | | | |
| ΔDGA1::IboH-LtaE-MCR-C | | + | | + | |
| ΔDGA1::ADC-MAO-MCR-C | | | + | | + |
| TAL titer (mg/L) | 2368.9 | 2401.4 | 2310.4 | 2822.6 | 2893.4 |
| scale | 250 mL baffled-flask | | | | |

**Fig. 5**. Feeding L-glutamate or L-aspartate to improve polyketide production in TAL-ILM or TAL-AMM strain. (**A**) TAL, HHEP and 3-HP production in TAL-ILM strain with or without feeding of 34 mM L-glutamate in 250 mL baffled-flask. (**B**) Growth fitness of HHEP-producing strain (TAL-AMM) is reduced compared to other TAL-producing strain; (**C**) TAL, HHEP and 3-HP production in TAL-AMM strain with or without feeding of 34 mM L-aspartate in 250 mL baffled-flask; (**D**) HPLC profile of TAL and HHEP from the engineered strains after knocking out HBD1; (**E**) TAL titer and specific TAL yield from the engineered strains with or without amino acid feeding in 250 mL baffled-flask. Experiments were performed in triplicate and the data is reported as mean ± SD. *** indicates statistically highly significant ($p < 0.001$), * indicates statistically significant ($p < 0.05$), ns indicates statistically significant ($p > 0.05$).

We next tested whether feeding of L-glutamate or L-aspartate to the ILM and AMM strains will boost TAL and HHEP titers. We initially tested the feeding experiment in 24-well plates, and both pathways failed to improve TAL or HHEP production. We speculated that oxygen availability may fall below the threshold necessary to drive efficient hydroxylation of L-glutamate or the oxidative deamination of β-alanine as L-glutamate or L-aspartate was fed to the deep-well culture. To improve oxygen supply, we cultivated the ILM strain in shaking flasks. After feeding 34 mM L-glutamate to the TAL-ILM strain, both TAL and HHEP titer were increased in the shaking flasks (**Fig. 5A**). TAL and 3HP yield were increased by 25%

269 and 29%, respectively, compared to the same strain without L-glutamate feeding (**Fig.**
270 **5A**, supplementary **Fig. S11A** and **Fig. S11C**). This result indicates the critical role of
271 $O_2$ to boost malonyl-CoA pools and polyketide synthesis in the TAL-ILM strain. HHEP
272 instead decreased after 72 hours (**supplementary Fig. S11B**), indicating the possible
273 degradation of HHEP by the host.

274 While cell fitness in the TAL-ILM, TAL-ACC and AMM strains remain unchanged,
275 the TAL-AMM strain exhibits pronounced growth-retardation (**Fig. 5B**), possibly due
276 to the inhibitory effect of HHEP. Using TAL as an internal standard, we determined
277 that TAL-AMM strain produced 3140.9 mg/L of HHEP (**Fig. 5C**). After feeding 34 mM
278 L-aspartate to TAL-AMM strain, the production of TAL, HHEP and 3HP increased by
279 17.4%, 14.7% and 55.5%, respectively (**Fig. 5C** and **Fig. S12B**). And the total
280 polyketide (both TAL and HHEP) was boosted to 5.0 g/L (**Fig. 5C**), which is more than
281 1.9-fold of the total polyketides (TAL and HHEP) than the ACC pathway (Fig. S1A).
282 HHEP is a structural analog of the natural product Kojic acid, which is a well-known
283 whitening and skincare natural product. This is the first report on the synthesis of the
284 nonnatural polyketide HHEP, and the biological activity of HHEP is yet to be
285 discovered.

286 We next deleted HBD1, to eliminate interference from the endogenous 3-HP-
287 CoA-related pathways (**Fig. 3B** and **3C**). Compared to TAL-AMM strain, the TAL-
288 ΔHBD1-AMM strain exhibited significantly lower HHEP production (**Fig. 5D** and
289 supplementary **Fig. S13A**). However, HHEP was still detectable in all the HBD1
290 knockout strain (**Fig. 5D**), suggesting that the precursor of HHEP, 3-hydroxypropanoyl-
291 CoA, may also be derived from the endogenous branched-chain amino acid
292 degradation (**Fig. 3B**). This highlights the complexity of metabolic networks and the
293 existence of alternative routes contributing to HHEP biosynthesis. Cell fitness analysis
294 (**Fig. S13B**) further revealed that deletion of HBD1 restored normal growth in the
295 TAL-AMM strain, indicating that HHEP may indeed act as a novel antimicrobial
296 compound. Thus, removal of HBD1 has enabled us to have a clear assessment of ILM
297 and AMM pathway performance.

298 To assess the efficiency of different malonyl-CoA pathways, we next constructed
299 three engineered strains based on HBD1-deleted chassis, the TAL-ΔHBD1-ACC strain
300 produced 2368.9 mg/L TAL, while the ILM and AMM strains yielded 2401.4 mg/L and
301 2310.4 mg/L, respectively. These results indicate that the ILM and AMM pathways
302 provide malonyl-CoA at a level comparable to that of ACC pathway (**Fig. 5E**). We next
303 fed 34 mM L-glutamate to the ILM strain, and TAL production was increased from

2401.4 mg/L to 2822.6 mg/L. Similarly, feeding 34 mM L-aspartate to the AMM strain raised TAL titer from 2310.4 mg/L to 2893.4 mg/L, corresponding to a 25.2% increase (**Fig. 5D** and **Fig. 5E**). These results confirm that the new amino acid-derived malonyl-CoA pathways effectively boosted polyketide production in *Y. lipolytica*.

### 2.5 Feeding L-aspartate to boost polyketide production in bioreactor

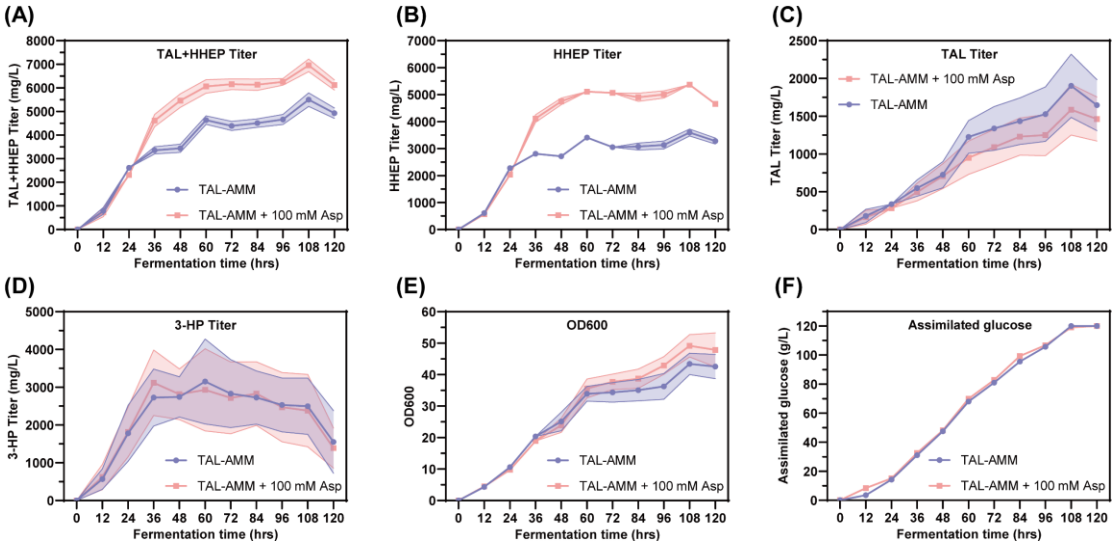


**Fig. 6** Feeding L-aspartate to improve polyketide production in TAL-AMM strain in a 1.0 L mini-bioreactor. TAL+HHEP(**A**), HHEP(**B**), TAL(**C**) and 3-HP(**D**) production in TAL-AMM strain with or without feeding of 100 mM L-aspartate in a 1L bioreactor; (**E**) Optical density OD600 during fermentation in a 1L bioreactor; (**F**) Amount of glucose consumed during fermentation in a 1L bioreactor.

To evaluate the effect of L-aspartate feeding on polyketide production at larger scale, we conducted a 1 L bioreactor fermentation using the TAL-AMM strain, with or without the addition of 100 mM L-aspartate. The combined titer of TAL and HHEP in the L-aspartate-fed culture reached a peak of 6955.2 mg/L at 108 h, which is a 26.4% increase compared to the maximum titer of 5500.5 mg/L in the control strain without L-aspartate feeding (**Fig. 6A**). This substantial improvement suggests that L-aspartate feeding enhances malonyl-CoA supply toward polyketide biosynthesis. With L-Asp feeding, HHEP reached a peak of 5368.6 mg/L, representing a 49.2% increase compared to the control group (3597.3 mg/L) (**Fig. 6B**). Notably, HHEP reached 5113.0 mg/L by 60 hours of fermentation, when only 70 g/L of glucose was consumed (**Fig. 6F**). HHEP accumulation slows down after 60 hours, despite continued glucose consumption. This may indicate a product feedback inhibition of the HHEP pathway.

Interestingly, TAL production was decreased in the L-aspartate-fed culture

329 compared to the control, particularly after 48 hours (**Fig. 6C**). This suggests that with
330 excess L-aspartate, a greater portion of the precursor malonyl-CoA is channeled
331 toward HHEP biosynthesis rather than TAL accumulation. The increased availability of
332 L-aspartate likely facilitates the formation of the HHEP precursor 3-hydroxypropionyl-
333 CoA (3-HP-CoA), thereby leading to substantial increase of HHEP. This shift in product
334 distribution reinforces the role of L-aspartate as a flux-enhancing agent that drives
335 carbon through the AMM pathway. Furthermore, the 3-HP titer in the L-aspartate-
336 fed culture peaked at 3119.0 mg/L, equivalent to 3152.2 mg/L maximum in the
337 control strain. Notably, 3-HP production gradually decreased after 60 hours,
338 regardless of whether or not L-aspartate was fed (**Fig. 6D**). This suggests a shift in
339 metabolic flux from 3-HP to HHEP: 3-HP was converted to 3-HP-CoA promoting an
340 increased flux toward HHEP.

341 Cell growth slightly improved with L-aspartate supplementation, reaching a final
342 OD600 of 49.2, compared to 43.4 in the control (**Fig. 6E**). Despite differences in
343 product profiles, glucose consumption was identical between both conditions, with a
344 total consumption of ~120 g/L at the end of fermentation (**Fig. 6F**). This indicates that
345 the observed differences in product titers were not due to changes in glucose uptake
346 but rather due to increased supply of malonyl-CoA through the amino-acid-derived
347 malonyl-CoA pathways.

348 Together, these results demonstrate that L-aspartate feeding is an effective
349 strategy to enhance high-value polyketide production in engineered *Y. lipolytica*. Both
350 L-aspartate and L-glutamate are among the most abundant amino acids in food
351 waste. Different from the reported transaminase-MCR route (*20*), our re-designed
352 malonyl-CoA pathway leverages hydroxylation (in the case ILM) or oxidative
353 deamination (in the case AMM) with oxygen consumption, and therefore it provides
354 a large driving force to compensate the relatively inefficient MCR step. When coupled
355 together, the novel ILM and AMM pathway efficiently converted L-glutamate or L-
356 aspartate to malonyl-CoA and improved the production of both TAL and HHEP. These
357 novel pathways are particularly useful to produce malonyl-CoA-derived compounds
358 under aerobic conditions, potentially benefiting large-scale fermentations. Our
359 results established a promising and scalable polyketide production platform from
360 low-cost amino acid precursors.

361 ## 3. Conclusions

362 Herein we have designed and validated two malonyl-CoA biosynthetic pathways
363 in *Y. lipolytica*, utilizing L-glutamate and L-aspartate as substrates. These pathways

364 provide an efficient and ATP-independent alternative for metabolic engineering
365 applications, which expands nature's capacity to produce malonyl-CoA-derived
366 chemicals in *Y. lipolytica*. By leveraging oxidative deamination and decarboxylation
367 reactions, both pathways effectively redirected metabolic flux toward malonyl-CoA,
368 significantly enhancing the biosynthesis of triacetic acid lactone (TAL) and a new-to-
369 nature polyketide HHEP. The strain with AMM pathway produced a novel polyketide
370 HHEP, at 5.4 g/L, highlighting the superior metabolic versatility of *Y. lipolytica*. The
371 total polyketide production reached 7.0 g/L in a 1L bioreactor. Our findings
372 demonstrated that low-cost amino acids or protein wastes could be used as efficient
373 raw materials to manufacture high value polyketides. The study also reveals
374 thermodynamic coupling could be used to overcome inefficient enzymatic steps.
375 Overall, this work represents an important step toward sustainable and cost-effective
376 production of polyketides by rewiring the amino acid metabolism in microbes.

377 
## 4. Materials and methods

378 
### 4.1 Strains and cultural conditions

379 All engineered *Y. lipolytica* strains in this research were derived from Po1fk.
380 *Escherichia coli* DH5α was cultured in LB medium supplemented with 100 mg/mL
381 ampicillin for plasmid construction and extraction. *Y. lipolytica* strains were cultured
382 in YPD medium for genomic DNA extraction or linearized plasmid transformation.
383 Engineered strains were fermented in YPD to produce triacetic acid lactone. SD-Ura
384 and SD-Leu plates were used to isolate positive *Y. lipolytica* transformants. Cre-loxP
385 system was used to eliminate the URA3 selection marker (*34*). To conduct 24-deep-
386 well plates or 250 mL shake-flask fermentation, the strain was grown in 3 mL YPD
387 medium for 1 day to prepare a seed culture. A portion of the seed culture was
388 utilized to inoculate 3.5 mL or 25 mL of YPD medium with 80 g/L glucose and
389 additional glutamic acid or aspartic acid, with the aim of achieving an initial OD600
390 value of 0.2, followed by fermentation at 30°C and 250 rpm for 96 h. All engineered
391 strains utilized in fermentation were prototrophic. The formulations of LB medium,
392 YPD medium, SD-Ura plate, SD-Leu plate, and YPD-5-FOA plate were outlined in the
393 **supplementary materials**.

394 
### 4.2 Genetic engineering and strain construction

395 In this research, expression cassette plasmids for individual genes were
396 generated by Gibson assembly and verified by DNA sequencing. Subsequently, we
397 assembled multiple expression cassettes on an integrative vector using a subcloning

398 method of digestion and ligation, following YaliBrick assembly protocols (*35, 36*). All
399 plasmids constructed are listed in the **supplementary Table S1**. The plasmid (*35*)
400 used for gene integration consists of two 1~1.5 kb homology arms, which correspond
401 to sequences 5'-upstream and 3'-downstream of the integration site, and a loxP-
402 URA3-loxP cassette, the latter of which was used to recover the URA3 screening
403 marker by using Cre-loxP recombination system. The plasmid used for gene
404 integration was inserted into the *Y. lipolytica* chromosome for gene overexpression.
405 Homology arms of integration sites, as well as terminators and promoters, were
406 amplified by PCR using the genomic DNA from strain Po1fk or other constructed
407 plasmids as templates. The exogenous gene coding sequences were codon-optimized
408 and synthesized by Genewiz (Suzhou, China). *Y. lipolytica* endogenous gene *Yl*ACC1
409 (YALI0C11407g) devoid of intron sequence was amplified through PCR utilizing the
410 genomic DNA of strain Po1fk as the template. The gene sequences that have been
411 codon optimized are provided in the **supplementary Table S2**. All cloning primers
412 and check primers are listed in **supplementary Table S3**.

413 **4.3 *Y. lipolytica* transformation and strain verifications**

414 The strain to be transformed was cultured in YPD medium for 24 hours, after
415 which the yeast cells were collected and resuspended in PBS buffer to wash away the
416 YPD medium. Subsequently, 50% PEG4000, 2 M lithium acetate, salmon sperm DNA,
417 and a linearized plasmid were added for homologous recombination transformation
418 (*37*). Positive clones were selected on CSM-Ura plates, and genomic DNA from the
419 clones was extracted using the Lysis Buffer with Microorganism Direct PCR Kit
420 (Takara, Beijing) for PCR-based identification. A single positive clone identified by PCR
421 was then inoculated in YPD medium for 24 hours and transformed with the pYLXP'-
422 Cre plasmid to eliminate the URA3 marker gene. The resulting colonies were streaked
423 on both YPD-5-FOA and CSM-Ura plates. Colonies that grew on YPD-5-FOA plates but
424 failed to grow on CSM-Ura plates were selected for PCR analysis to confirm the
425 successful elimination of the URA3 marker gene. Strains lacking the URA3 marker
426 gene were then subjected to another round of linearized plasmid transformation and
427 screening. All strains constructed in this work are listed in **supplementary Table S4**.

428 **4.4 Dry cell weight quantification and triacetic acid lactone extraction**

429 The cell growth was monitored by measuring the optical density at 600 nm
430 (OD600) with a UV–vis spectrophotometer that could also be converted to dry cell
431 weight (DCW) according to the calibration curve (DCW: OD600 = 0.33:1 (g/L). The
432 fermentation broth was centrifuged at 12,000 rpm for 3 min and the culture was

433 used for analyzing the concentration of TAL. For complete extraction of TAL, 100 μL
434 fermentation culture was resuspended in 700 μL of ultrapure water containing plastic
435 particles as abrasives. The cell culture was grinded using a cryo-grinding machine at -
436 20 °C for 20 cycles of 40 s each, followed by centrifugation at 12,000 rpm for 3 min.
437 After the mixture was centrifuged, the supernatant was taken for high performance
438 liquid chromatography (HPLC) analysis.

439 **4.5 Characterization and quantification of TAL, 3-HP, and unknown peak**

440 An Agilent 1260 Infinity II instrument was utilized for HPLC analysis, with a
441 variable wavelength detector (VWD) and a C18 column (4.6 mm × 100 mm). The
442 HPLC analysis was carried out using a mobile phase consisting of solvent A (0.1%
443 formic acid in water) and solvent B (methanol). A gradient elution was applied
444 starting with 10% B, increasing to 100% B over 20 minutes, followed by 3 minutes at
445 100% B. The flow rate was 1.0 mL/min, with a column temperature of 30°C.
446 Detection was performed at 280 nm, and the injection volume was 10 μL (*38*).
447 Retention time of triacetic acid lactone is about 5.2 min. The HPLC analysis for 3-
448 hydroxypropionate (3-HP) was carried out using a single mobile phase (0.1% formic
449 acid in water - methanol (95:5, v/v) mixture), and the total elution time was 10
450 minutes. The flow rate was 1.0 mL/min, with a column temperature of 30°C.
451 Detection was performed at 210 nm for 3-HP, and the injection volume was 10 μL.
452 Retention time of 3-HP is about 3.0 min. TAL and 3-HP standard was purchased from
453 Macklin, China.

454 The unknown compound was characterized by using a Thermo Scientific Q
455 Extractive mass spectrometer equipped with an electrospray ionization (ESI) source
456 operated in both positive and negative ionization mode. Full-scan mass spectra were
457 acquired over a range of m/z 50–500. ESI parameters were optimized as follows: the
458 spray voltage 3500 V, capillary temperature 350 °C, sheath gas 30 Arb, aux gas 10
459 Arb, probe heater temp 325 °C. Chromatographic separation was achieved using a
460 C18 column (2.1 mm × 100 mm) with a flow rate of 0.5 mL/min and an injection
461 volume of 5 μL, following the same mobile phase composition and gradient elution
462 program as the HPLC method.

463 Statistical analysis of metabolite titer and content was conducted using Student's
464 t-test, and the significances were defined as: $P > 0.05$ (ns), $P < 0.05$ (*), $P < 0.01$ (**),
465 $P < 0.001$ (***). Each value represents the mean ± standard deviation from at least
466 three independent experiments ($n > 3$).

## Author contributions

Jinpeng Wang: Conceptualization, Methodology, Writing - original draft, Visualization. Yuxiang Hong: Data curation, Visualization, Investigation. Zizhao Wu: Methodology, Investigation, Data analysis. Ayelet Fishman: Writing - review & editing. Peng Xu: Conceptualization, Writing - review & editing, Project administration, Funding acquisition.

## Data availability

Data will be made available on reasonable request.

## Acknowledgements

This work was financially supported by the National Natural Science Foundation of China (22378083), Guangdong Provincial Key Laboratory of Materials and Technologies for Energy Conversion (MATEC), and Muyuan laboratory (Program ID: 12106022401).

480 **Table 1**. Summary of the reaction components of canonical (**a**, **b**), noncanonical (**c**) and the new predicted malonyl-CoA (**d** and **e**) pathways.

| Pathway | | Reaction | Cofactor | ATP consume | $CO_2$ release | Redox balance | Enzyme | EC | Source |
|---|---|---|---|---|---|---|---|---|---|
| Canonical | a | Pyruvate + CoASH + NAD <=> Acetyl-CoA + NADH + CO2 | CoASH,NAD+ | 0 | 1 | NADH | **PDH** | **1.2.1.51** | Tong, L. (2005) (*16*) |
| | | Acetyl-CoA + ATP + CO2 + H2O <=> ADP + Malonyl-CoA + Pi | NA | 1 | 0 | 0 | **ACC** | **6.4.1.2** | |
| | b | Malonate + CoASH + ATP +H2O <=> AMP + Malonyl-CoA + 2Pi | CoASH | 2 | 0 | 0 | **MS** | **6.2.1.76** | Wakil, S. J. (1958) (*19*) |
| Noncanonical | c | beta-Alanine + Pyruvate <=> alpha-Alanine + Malonate semialdehyde | NA | 0 | 0 | 0 | **TA(BauA)** | **2.6.1.18** | Li, J., et al. (2024) (*20*) |
| | | Malonate semialdehyde + CoASH + NADP <=> Malonyl-CoA + NADPH | CoASH,NADP+ | 0 | 0 | NADPH | **MCR-C** | **1.2.1.75** | |
| Predicted | d | L-glutamate + 2-oxoglutarate + O2 <=> 3-hydroxy-L-glutamate + succinate + CO2 | NA | 0 | 1 | 0 | **IboH** | **1.14.11.76** | Obermaier, S., et al. (2020)(*21*), Nie, M., et al. (2024) (*22*) |
| | | 3-Hydroxy-L-glutamate <=> Malonate semialdehyde + Glycine | NA | 0 | 0 | 0 | **Aldolase** | **4.1.2.48** | |
| | | Malonate semialdehyde + CoASH + NADP <=> Malonyl-CoA + NADPH | CoASH,NADP+ | 0 | 0 | NADPH | **MCR** | **1.2.1.75** | |
| | e | Aspartate <=> beta-Alanine + CO2 | NA | 0 | 1 | 0 | **ADC** | **4.1.1.11** | Cronan, J., et al. (1980)(*23*), Yamashita, M., et al. (1996) (*24*) |
| | | beta-Alanine + H2O+ O2 <=> Malonate semialdehyde + H2O2 + NH3 | NA | 0 | 0 | 0 | **MAO** | **1.4.3.21** | |
| | | Malonate semialdehyde + CoASH + NADP <=> Malonyl-CoA + NADPH | CoASH,NADP+ | 0 | 0 | NADPH | **MCR** | **1.2.1.75** | |

481

482

483 **Table 2.** Summary of thermodynamic and kinetic parameters of canonical, noncanonical and the novel malonyl-CoA pathways.

| Pathway | | Reaction | eQuilibrator 3.0 | | | | BRENDA | | UniKP (Prediction) | | |
|---|---|---|---|---|---|---|---|---|---|---|---|
| | | | $\Delta_rG'^m$ [kJ/mol] | $\Delta_rG'^m$(total) [kJ/mol] | $\Delta_rG'^o$ [kJ/mol] | $\Delta_rG'^o$(total) [kJ/mol] | $K'_{eq}$ | $K_m$ (mM) | $k_{cat}$(1/s) | $K_m$(mM) | $k_{cat}/K_m$(1/mMs) |
| Canonical | a | Pyruvate + CoA-SH + NAD <=> Acetyl-CoA + NADH + CO2 | -34.2 ± 6.3 | -51.3 | -34.2 ± 6.4 | -51.3 | 1.0 × 10^6 | 0.027 - 0.21 | 7.08 | 0.91 | 7.77 |
| | | Acetyl-CoA + ATP + CO2 + H2O <=> ADP + Malonyl-CoA + Pi | -17.1 ± 6.2 | | -17.1 ± 6.3 | | 1.0 × 10^3 | 0.0002 - 1.2 | 4.90 | 0.04 | 123.00 |
| | b | Malonate + CoA-SH + ATP +H2O <=> AMP + Malonyl-CoA + 2Pi | -53.4 ± 2.9 | -53.4 | -36.3 ± 2.9 | -36.3 | 2.3 × 10^6 | 0.0368 - 8.7 | 5.53 | 0.38 | 14.53 |
| Noncanonical | c | beta-Alanine + Pyruvate <=> alpha-Alanine + Malonate semialdehyde | -3.7 ± 5.7 | 0.6 | -3.7 ± 5.7 | -16.5 | 4 | 1.1 - 14 | 0.96 | 3.47 | 0.28 |
| | | Malonate semialdehyde + CoA-SH + NADP <=> Malonyl-CoA + NADPH | 4.3 ± 8.8 | | -12.8 ± 8.8 | | 1.8 × 10^2 | NA | 2.96 | 0.57 | 5.17 |
| Predicted | d | L-glutamate + 2-oxoglutarate + O2 <=> 3-hydroxy-L-glutamate + succinate + CO2 | -444.0 ± 10.2 | -466.6 | -444.0 ± 10.2 | -466.6 | 6.7 × 10^77 | NA | 5.08 | 0.86 | 5.90 |
| | | 3-Hydroxy-L-glutamate <=> Malonate semialdehyde + Glycine | -26.9 ± 9.2 | | -9.8 ± 9.2 | | 50 | NA | 2.41 | 0.71 | 3.38 |
| | | Malonate semialdehyde + CoA-SH + NADP <=> Malonyl- | 4.3 ± 8.8 | | -12.8 ± 8.8 | | 1.8 × 10^2 | NA | 2.96 | 0.57 | 5.17 |

| | | | | | | | | | | |
|---|---|---|---|---|---|---|---|---|---|---|
| | CoA + NADPH | | | | | | | | | |
| e | Aspartate <=> beta-Alanine + CO2 | -34.0 ± 11.7 | -146.3 | -16.9 ± 11.7 | -129.2 | 9.1 × 10^2 | 0.151 - 3.18 | 6.90 | 0.57 | 12.09 |
| | beta-Alanine + H2O+ O2 <=> Malonate semialdehyde + H2O2 + NH3 | -116.6 ± 10.1 | | -99.5 ± 10.1 | | 2.8 × 10^17 | 0.00088 - 12.8 | 12.70 | 0.64 | 19.82 |
| | Malonate semialdehyde + CoASH + NADP <=> Malonyl-CoA + NADPH | 4.3 ± 8.8 | | -12.8 ± 8.8 | | 1.8 × 10^2 | NA | 2.96 | 0.57 | 5.17 |

484 ## References


485 1. Z. Xue *et al.*, Production of omega-3 eicosapentaenoic acid by metabolic
486 engineering of Yarrowia lipolytica. *Nature biotechnology* **31**, 734-740 (2013).
487 2. K. Qiao, T. M. Wasylenko, K. Zhou, P. Xu, G. Stephanopoulos, Lipid production in
488 Yarrowia lipolytica is maximized by engineering cytosolic redox metabolism. *Nature*
489 *biotechnology* **35**, 173-177 (2017).
490 3. P. Xu, K. Qiao, W. S. Ahn, G. Stephanopoulos, Engineering Yarrowia lipolytica as a
491 platform for synthesis of drop-in transportation fuels and oleochemicals.
492 *Proceedings of the National Academy of Sciences* **113**, 10848–10853 (2016).
493 4. L. Milke, J. Marienhagen, Engineering intracellular malonyl-CoA availability in
494 microbial hosts and its impact on polyketide and fatty acid synthesis. *Applied*
495 *microbiology and biotechnology* **104**, 6057-6065 (2020).
496 5. Z. Tan, J. M. Clomburg, S. Cheong, S. Qian, R. Gonzalez, A polyketoacyl-CoA
497 thiolase-dependent pathway for the synthesis of polyketide backbones. *Nature*
498 *Catalysis* **3**, 593-603 (2020).
499 6. K. A. Markham *et al.*, Rewiring Yarrowia lipolytica toward triacetic acid lactone for
500 materials generation. *Proceedings of the National Academy of Sciences* **115**, 2096-
501 2101 (2018).
502 7. P. Xu, S. Ranganathan, Z. L. Fowler, C. D. Maranas, M. A. G. Koffas, Genome-
503 scale metabolic network modeling results in minimal interventions that cooperatively
504 force carbon flux towards malonyl-CoA. *Metabolic engineering* **13**, 578-587 (2011).
505 8. Y. Lv, M. Marsafari, M. Koffas, J. Zhou, P. Xu, Optimizing Oleaginous Yeast Cell

506 Factories for Flavonoids and Hydroxylated Flavonoids Biosynthesis. *ACS synthetic*
507 *biology* **8**, 2514-2523 (2019).
508 9. Q. Dan *et al.*, A polyketide-based biosynthetic platform for diols, amino alcohols and
509 hydroxy acids. *Nature Catalysis* **8**, 147-161 (2025).
510 10. N. Lee *et al.*, Retrobiosynthesis of unnatural lactams via reprogrammed polyketide
511 synthase. *Nature Catalysis* **8**, 389-402 (2025).
512 11. W. Wang *et al.*, Harnessing the intracellular triacylglycerols for titer improvement of
513 polyketides in Streptomyces. *Nature biotechnology* **38**, 76-83 (2020).
514 12. X. Luo *et al.*, Complete biosynthesis of cannabinoids and their unnatural analogues
515 in yeast. *Nature* **567**, 123-126 (2019).
516 13. J. Ma, Y. Gu, P. Xu, Biosynthesis of cannabinoid precursor olivetolic acid in
517 genetically engineered Yarrowia lipolytica. *Communications Biology* **5**, 1239 (2022).
518 14. W. Zha, S. B. Rubin-Pitel, Z. Shao, H. Zhao, Improving cellular malonyl-CoA level in
519 Escherichia coli via metabolic engineering. *Metabolic engineering* **11**, 192-198
520 (2009).
521 15. A. O. Johnson *et al.*, Design and application of genetically-encoded malonyl-CoA
522 biosensors for metabolic engineering of microbial cell factories. *Metabolic*
523 *engineering* **44**, 253-264 (2017).
524 16. L. Tong, Acetyl-coenzyme A carboxylase: crucial metabolic enzyme and attractive
525 target for drug discovery. *Cellular and Molecular Life Sciences CMLS* **62**, 1784-1803
526 (2005).
527 17. S. H. Klass *et al.*, Engineering controllable alteration of malonyl-CoA levels to

528 enhance polyketide production. *Nature Chemical Biology* **21**, 1214-1225 (2025).

529 18. C. E. Bowman, M. J. Wolfgang, Role of the malonyl-CoA synthetase ACSF3 in
530 mitochondrial metabolism. *Advances in Biological Regulation* **71**, 34-40 (2019).

531 19. S. J. Wakil, A MALONIC ACID DERIVATIVE AS AN INTERMEDIATE IN FATTY
532 ACID SYNTHESIS. *Journal of the American Chemical Society* **80**, 6465-6465 (1958).

533 20. J. Li *et al.*, A non-carboxylative route for the efficient synthesis of central metabolite
534 malonyl-CoA and its derived products. *Nature Catalysis* **7**, 361-374 (2024).

535 21. S. Obermaier, M. Müller, Ibotenic Acid Biosynthesis in the Fly Agaric Is Initiated by
536 Glutamate Hydroxylation. *Angewandte Chemie International Edition* **59**, 12432-
537 12435 (2020).

538 22. M. Nie, J. Wang, K. Zhang, Engineering a Novel Acetyl-CoA Pathway for Efficient
539 Biosynthesis of Acetyl-CoA-Derived Compounds. *ACS synthetic biology* **13**, 358-369
540 (2024).

541 23. J. E. Cronan, Beta-alanine synthesis in Escherichia coli. *Journal of Bacteriology* **141**,
542 1291-1297 (1980).

543 24. M. Yamashita *et al.*, maoB, a gene that encodes a positive regulator of the
544 monoamine oxidase gene (maoA) in Escherichia coli. *Journal of Bacteriology* **178**,
545 2941-2947 (1996).

546 25. H. Yu, H. Deng, J. He, J. D. Keasling, X. Luo, UniKP: a unified framework for the
547 prediction of enzyme kinetic parameters. *Nature communications* **14**, 8211 (2023).

548 26. M. E. Beber *et al.*, eQuilibrator 3.0: a database solution for thermodynamic constant
549 estimation. *Nucleic Acids Research* **50**, D603-D609 (2022).

550 27. B. Niebel, S. Leupold, M. Heinemann, An upper limit on Gibbs energy dissipation
551 governs cellular metabolism. *Nature Metabolism* **1**, 125-132 (2019).
552 28. X. Yang *et al.*, Physical bioenergetics: Energy fluxes, budgets, and constraints in
553 cells. *Proceedings of the National Academy of Sciences* **118**, e2026786118 (2021).
554 29. E. Schrödinger, *What is life?: The physical aspect of the living cell*. (University
555 Press, Dhaka, Bangladesh, 1945), pp. 1 online resource (viii, 91 pages, IV plates on
556 92 leaves illustrations).
557 30. S. Eckermann *et al.*, New pathway to polyketides in plants. *Nature* **396**, 387-390
558 (1998).
559 31. J. M. Jez *et al.*, Structural control of polyketide formation in plant-specific polyketide
560 synthases. *Chemistry & Biology* **7**, 919-930 (2000).
561 32. I. Borodina *et al.*, Establishing a synthetic pathway for high-level production of 3-
562 hydroxypropionic acid in Saccharomyces cerevisiae via β-alanine. *Metabolic*
563 *engineering* **27**, 57-64 (2015).
564 33. A. J. Winter *et al.*, Programmed Iteration Controls the Assembly of the Nonanoic
565 Acid Side Chain of the Antibiotic Mupirocin. *Angewandte Chemie International*
566 *Edition* **61**, e202212393 (2022).
567 34. Y. Lv, H. Edwards, J. Zhou, P. Xu, Combining 26s rDNA and the Cre-loxP System
568 for Iterative Gene Integration and Efficient Marker Curation in Yarrowia lipolytica.
569 *ACS synthetic biology* **8**, 568-576 (2019).
570 35. L. Wong, J. Engel, E. Jin, B. Holdridge, P. Xu, YaliBricks, a versatile genetic toolkit
571 for streamlined and rapid pathway engineering in Yarrowia lipolytica. *Metabolic*

572 *Engineering Communications* **5**, 68-77 (2017).

573 36. L. Wong, B. Holdridge, J. Engel, P. Xu, in *Microbial Metabolic Engineering: Methods*
574 *and Protocols,* C. N. S. Santos, P. K. Ajikumar, Eds. (Springer New York, New York,
575 NY, 2019), pp. 155-177.

576 37. D. C. Chen, J. M. Beckerich, C. Gaillardin, One-step transformation of the dimorphic
577 yeast Yarrowia lipolytica. *Applied microbiology and biotechnology* **48**, 232-235
578 (1997).

579 38. H. Liu, M. Marsafari, F. Wang, L. Deng, P. Xu, Engineering acetyl-CoA metabolic
580 shortcut for eco-friendly production of polyketides triacetic acid lactone in Yarrowia
581 lipolytica. *Metabolic engineering* **56**, 60-68 (2019).

582

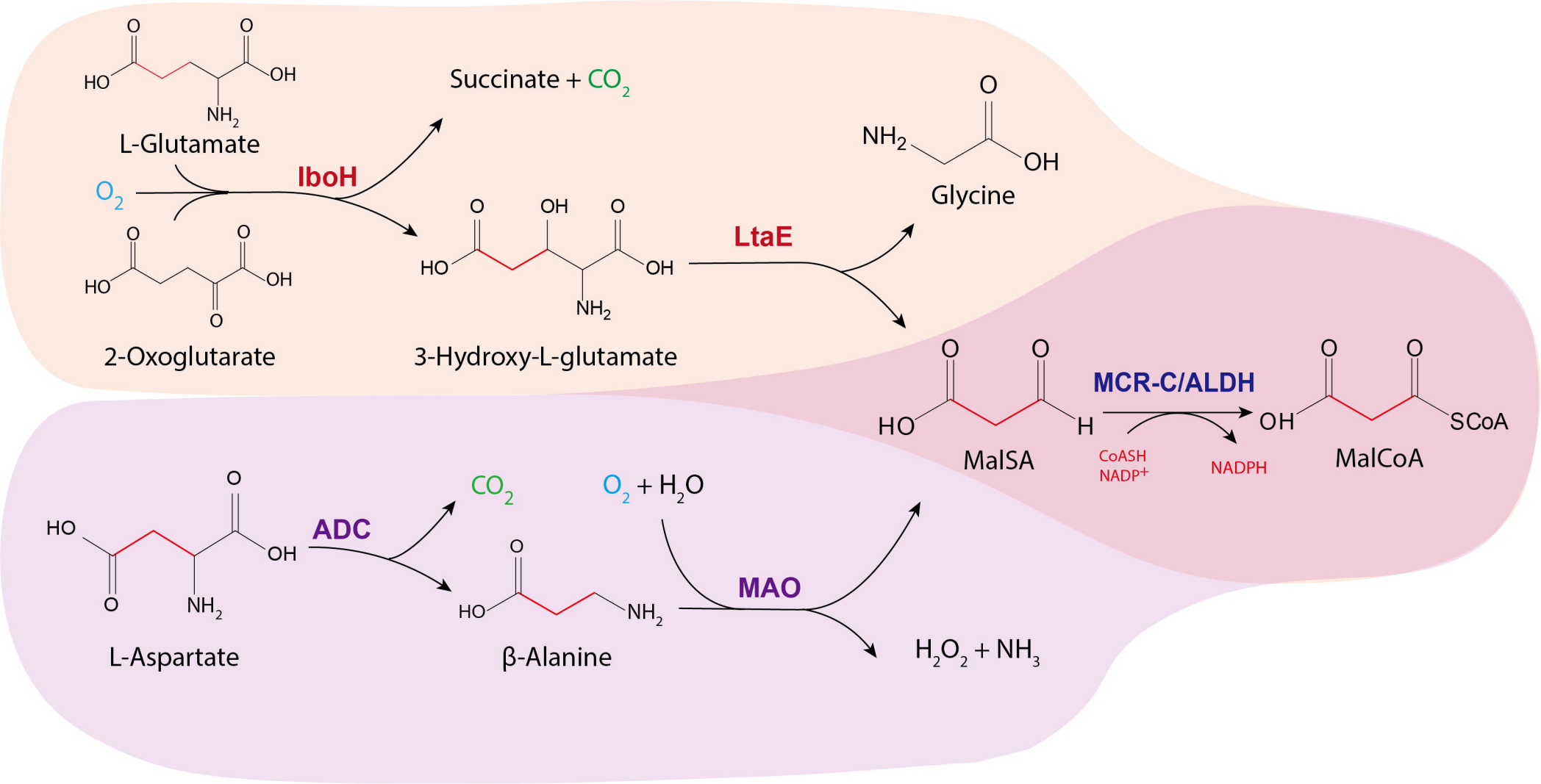
L-Glutamate
$O_2$
IboH
Succinate + $CO_2$
2-Oxoglutarate
3-Hydroxy-L-glutamate
LtaE
Glycine
MalSA
MCR-C/ALDH
CoASH
$NADP^+$
NADPH
MalCoA
L-Aspartate
ADC
$CO_2$
β-Alanine
$O_2 + H_2O$
MAO
$H_2O_2 + NH_3$

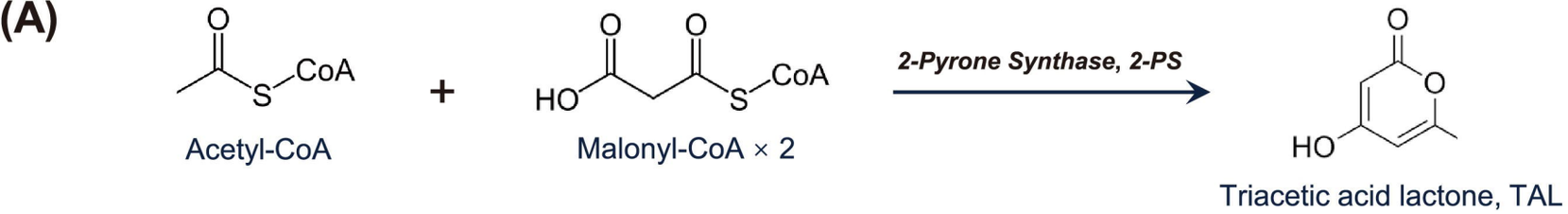


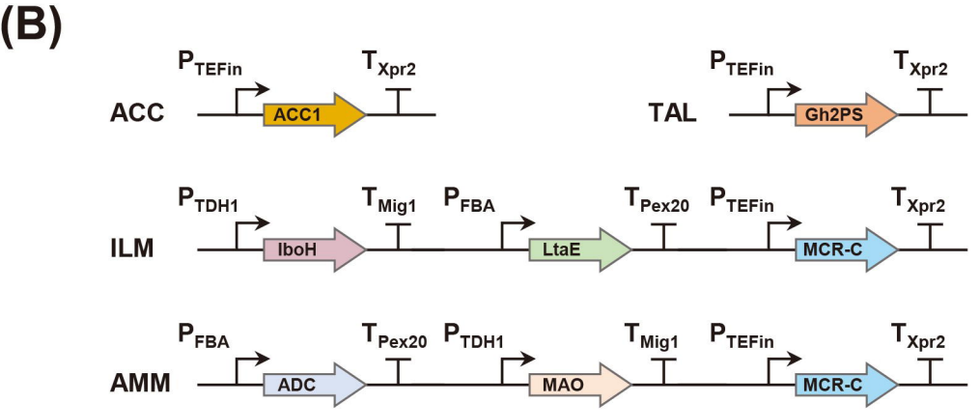


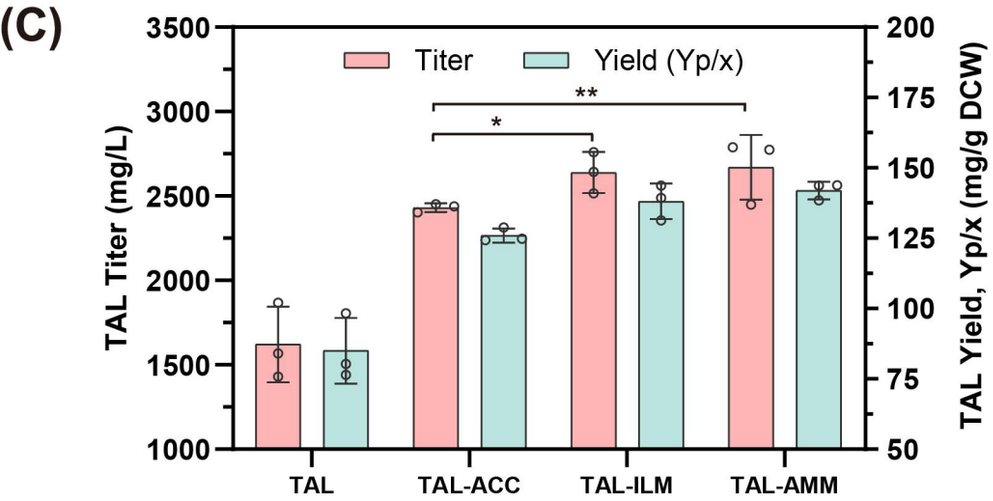


| | | | | |
|---|---|---|---|---|
| ΔLip1::**Gh2PS** | + | + | + | + |
| ΔDGA1::**ACC1** | | + | | |
| ΔDGA1::**IboH-LtaE-MCR-C** | | | + | |
| ΔDGA1::**ADC-MAO-MCR-C** | | | | + |
| **TAL titer (mg/L)** | 1621.3 | 2431.1 | 2638.8 | 2669.6 |
| **Scale** | 24 deep-well plate | | | |

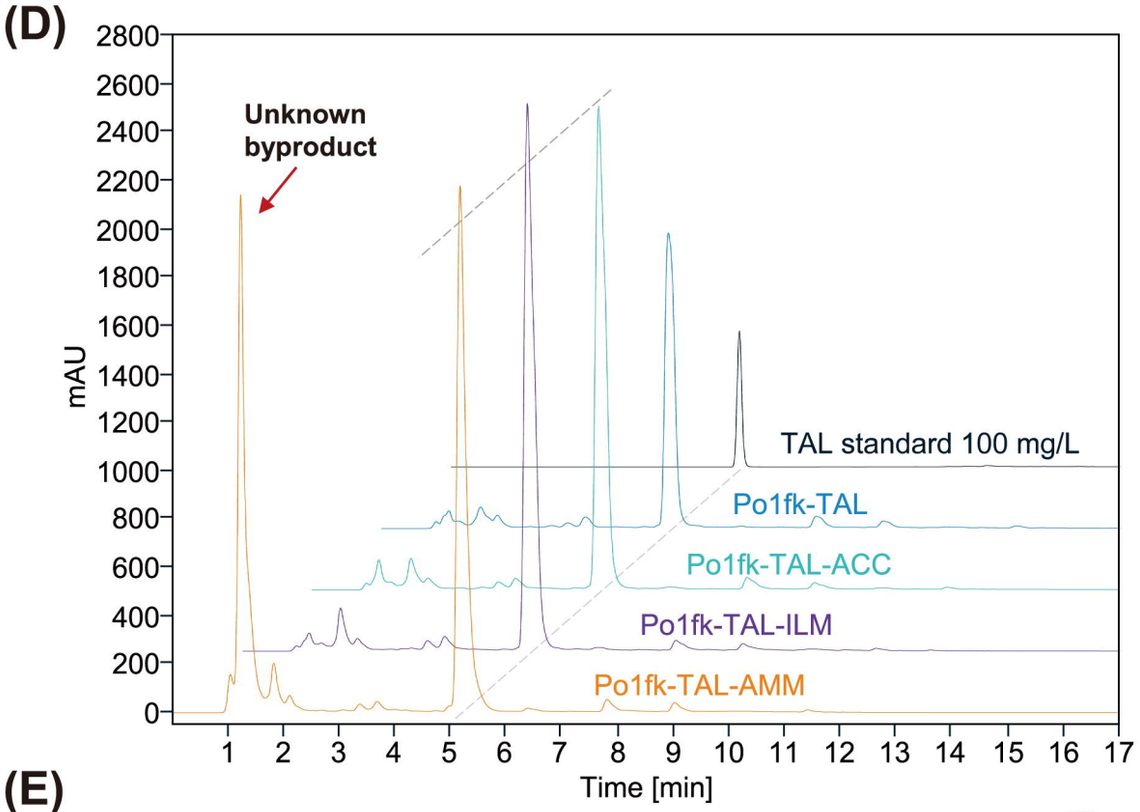


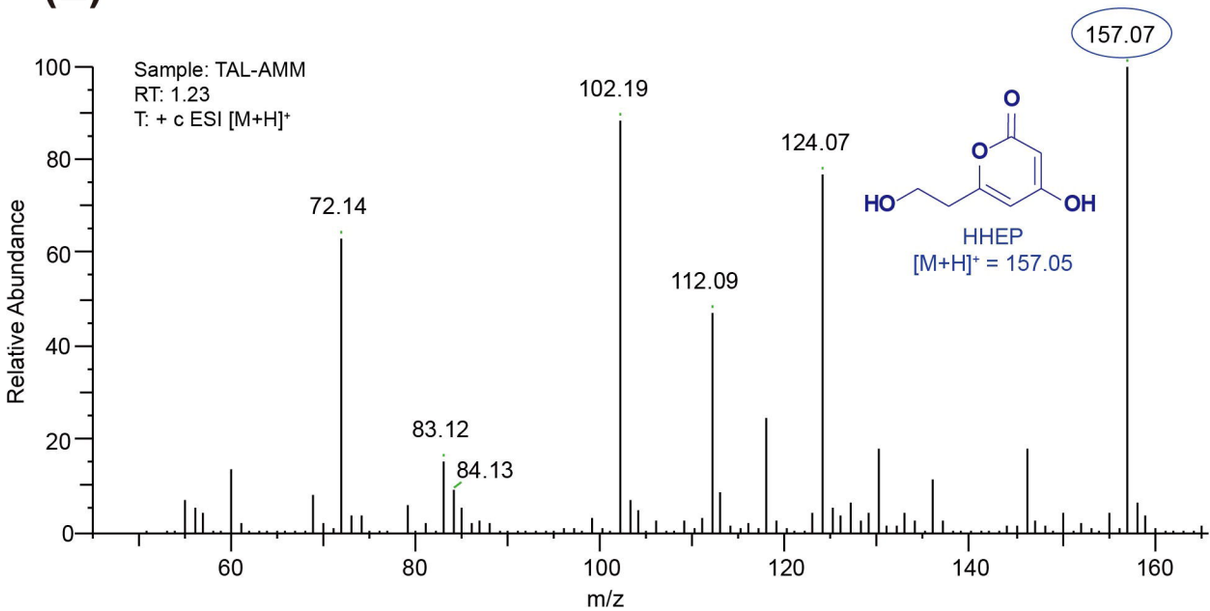

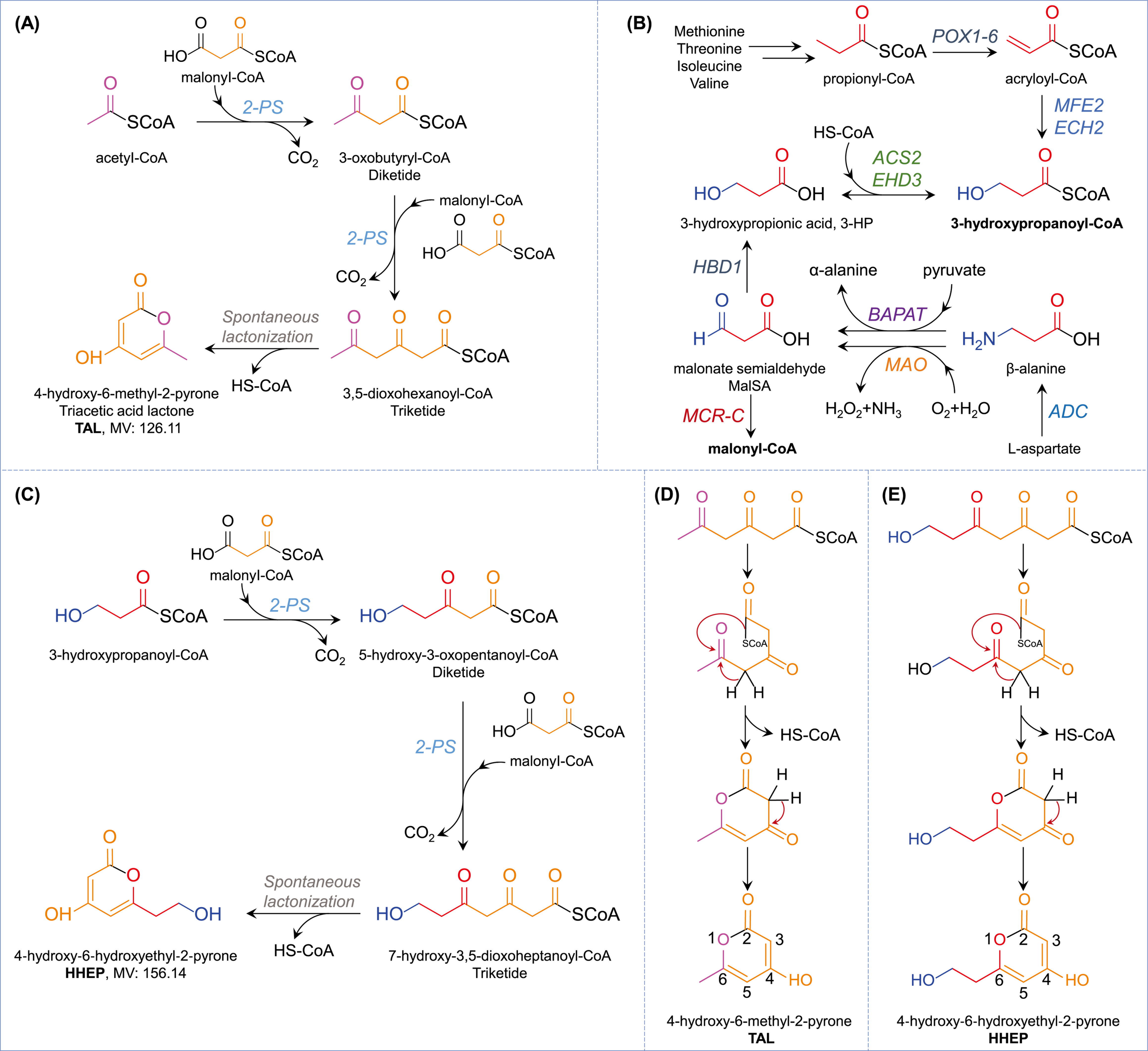
(A)
malonyl-CoA
acetyl-CoA
2-PS
CO2
3-oxobutyryl-CoA
Diketide
malonyl-CoA
2-PS
CO2
Spontaneous lactonization
HS-CoA
4-hydroxy-6-methyl-2-pyrone
Triacetic acid lactone
TAL, MV: 126.11
3,5-dioxohexanoyl-CoA
Triketide
(B)
Methionine
Threonine
Isoleucine
Valine
propionyl-CoA
POX1-6
acryloyl-CoA
MFE2
ECH2
HS-CoA
ACS2
EHD3
3-hydroxypropionic acid, 3-HP
3-hydroxypropanoyl-CoA
HBD1
α-alanine
pyruvate
BAPAT
MAO
malonate semialdehyde
MalSA
β-alanine
H2O2+NH3
O2+H2O
MCR-C
ADC
malonyl-CoA
L-aspartate
(C)
malonyl-CoA
3-hydroxypropanoyl-CoA
2-PS
CO2
5-hydroxy-3-oxopentanoyl-CoA
Diketide
malonyl-CoA
2-PS
CO2
Spontaneous lactonization
HS-CoA
4-hydroxy-6-hydroxyethyl-2-pyrone
HHEP, MV: 156.14
7-hydroxy-3,5-dioxoheptanoyl-CoA
Triketide
(D)
HS-CoA
4-hydroxy-6-methyl-2-pyrone
TAL
(E)
HS-CoA
4-hydroxy-6-hydroxyethyl-2-pyrone
HHEP

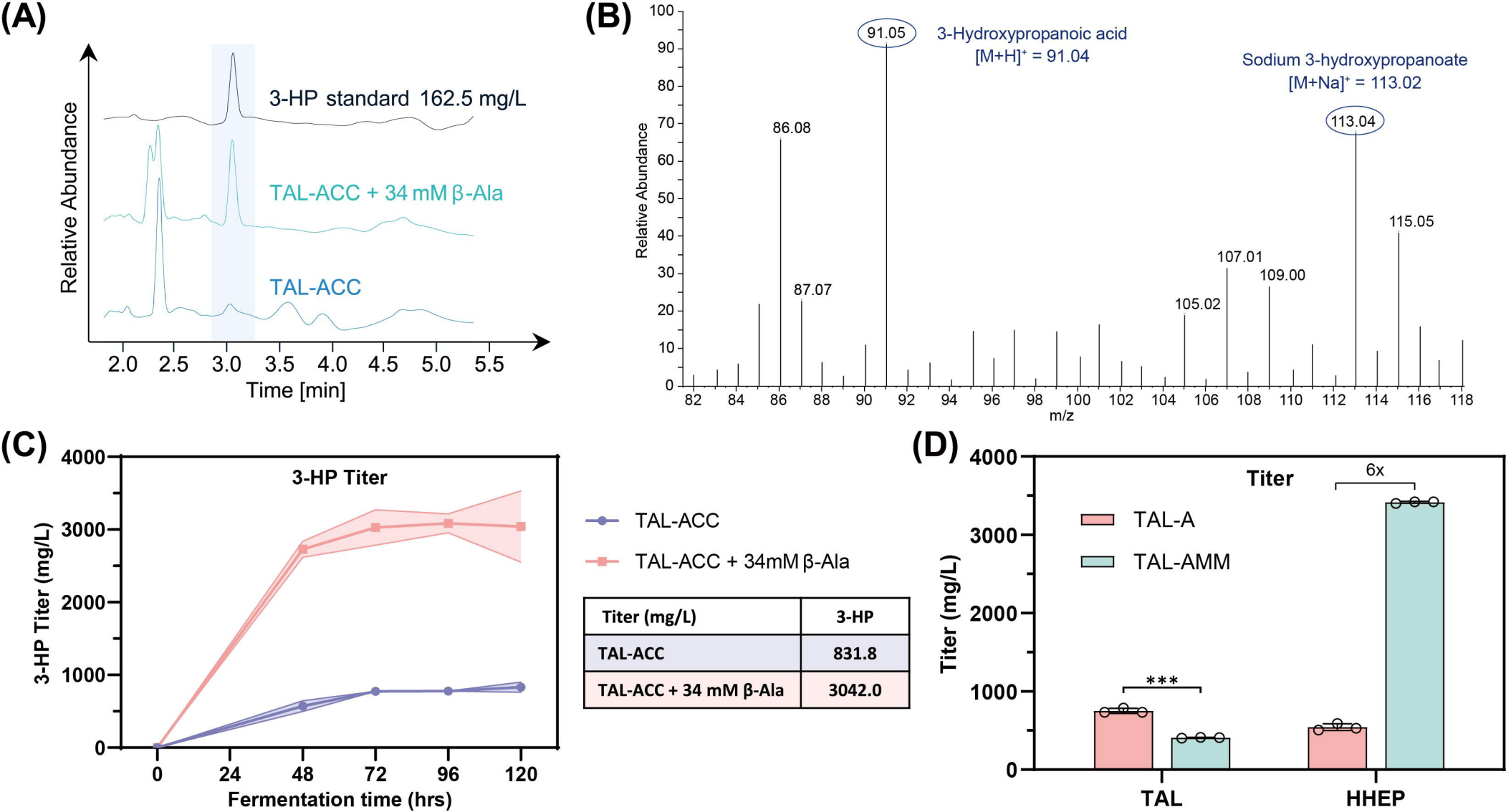


| Titer (mg/L) | 3-HP |
|---|---|
| TAL-ACC | 831.8 |
| TAL-ACC + 34 mM β-Ala | 3042.0 |

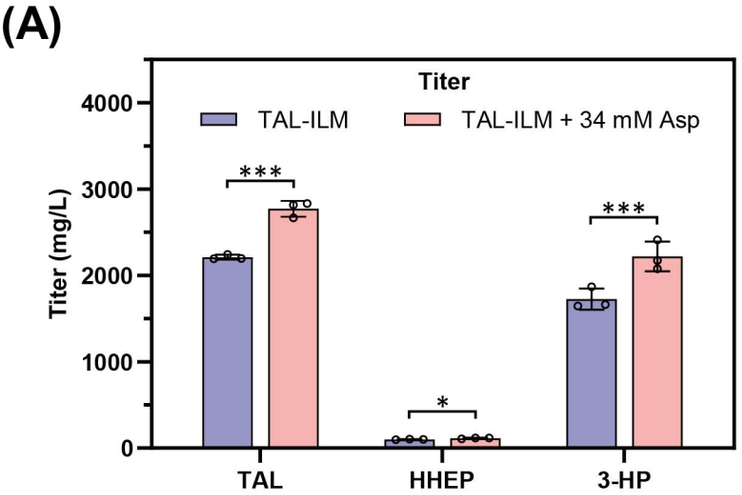


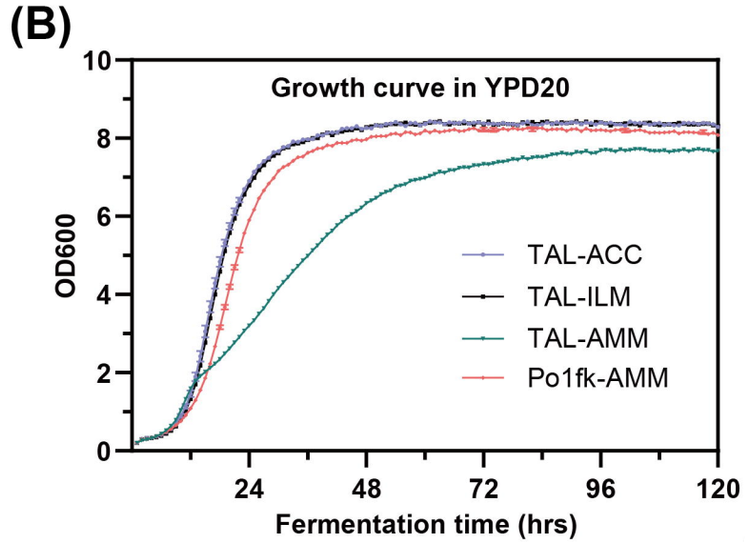


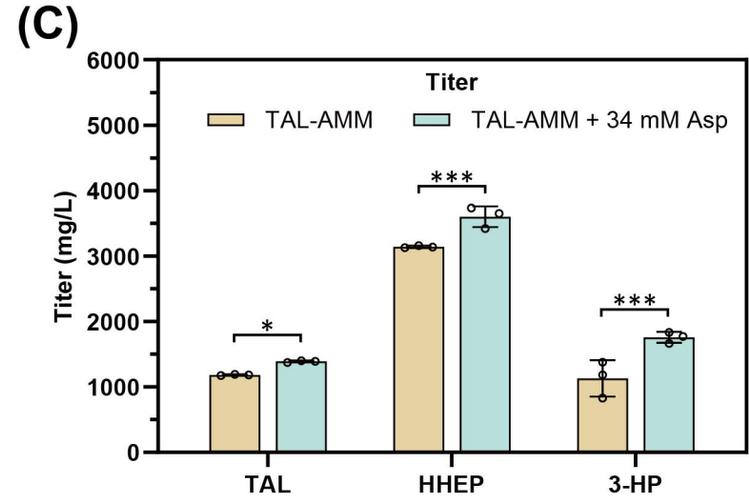


| Titer (mg/L) | TAL | HHEP | 3-HP |
|---|---|---|---|
| TAL-ILM | 2211.4 | 99.9 | 1726.2 |
| TAL-ILM + 34 mM Glu | 2772.7 | 113.9 | 2221.0 |

| Titer (mg/L) | TAL | HHEP | TAL+HHEP | 3-HP |
|---|---|---|---|---|
| TAL-AMM | 1182.8 | 3140.9 | 4323.7 | 1130.4 |
| TAL-AMM + 34 mM Asp | 1388.5 | 3601.1 | 4989.6 | 1757.4 |

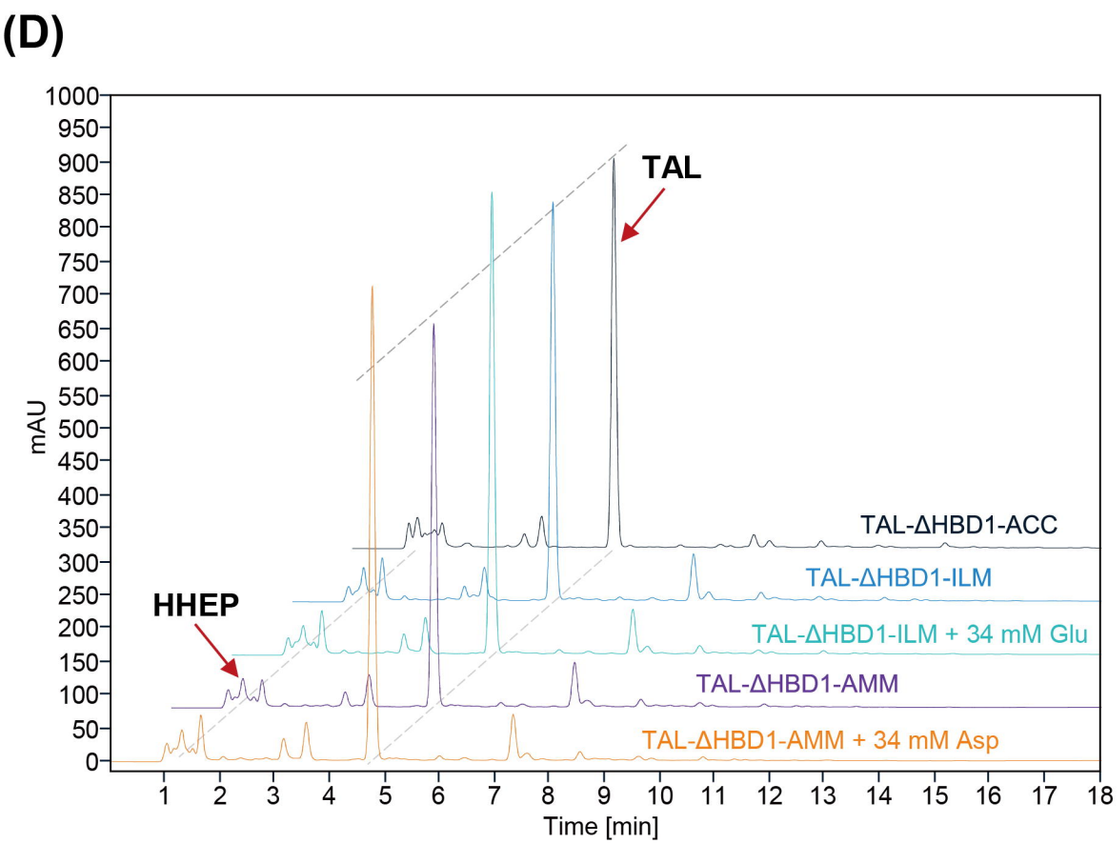


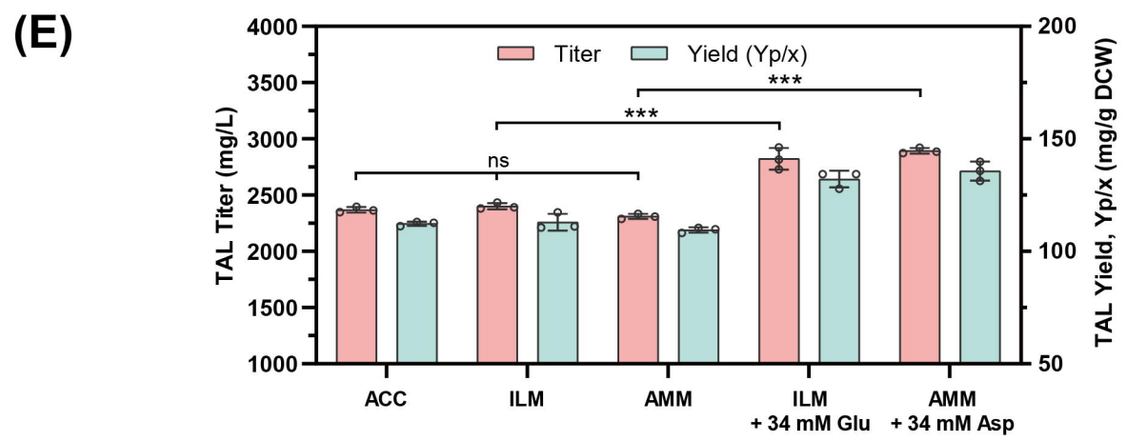


| | | | | | |
|---|---|---|---|---|---|
| ΔLip1::**Gh2PS** **ΔHBD1** | + + | + + | + + | + + | + + |
| ΔDGA1::**ACC1** | + | | | | |
| ΔDGA1::**IboH-LtaE-MCR-C** | | + | | + | |
| ΔDGA1::**ADC-MAO-MCR-C** | | | + | | + |
| **TAL titer (mg/L)** | 2368.9 | 2401.4 | 2310.4 | 2822.6 | 2893.4 |
| **scale** | 250 mL baffled-flask | | | | |

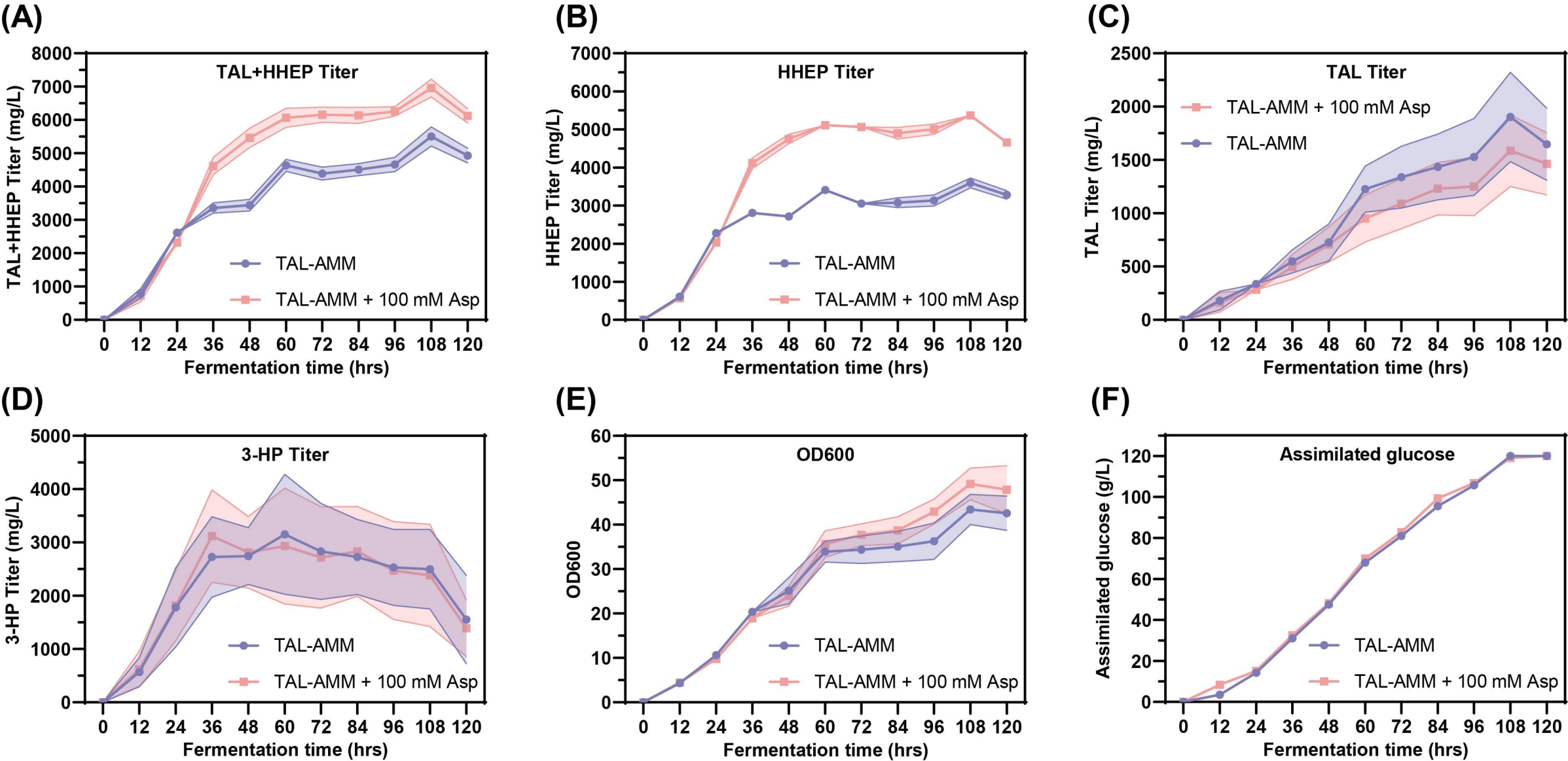
(A)
TAL+HHEP Titer
TAL+HHEP Titer (mg/L)
Fermentation time (hrs)
TAL-AMM
TAL-AMM + 100 mM Asp
(B)
HHEP Titer
HHEP Titer (mg/L)
Fermentation time (hrs)
TAL-AMM
TAL-AMM + 100 mM Asp
(C)
TAL Titer
TAL Titer (mg/L)
Fermentation time (hrs)
TAL-AMM + 100 mM Asp
TAL-AMM
(D)
3-HP Titer
3-HP Titer (mg/L)
Fermentation time (hrs)
TAL-AMM
TAL-AMM + 100 mM Asp
(E)
OD600
OD600
Fermentation time (hrs)
TAL-AMM
TAL-AMM + 100 mM Asp
(F)
Assimilated glucose
Assimilated glucose (g/L)
Fermentation time (hrs)
TAL-AMM
TAL-AMM + 100 mM Asp